Optical Engineering

SPIEDigitalLibrary.org/oe

Airborne Aero-Optics Laboratory

Eric J. Jumper
Michael A. Zenk
Stanislav Gordeyev
David Cavalieri
Matthew R. Whiteley

Airborne Aero-Optics Laboratory

Eric J. Jumper
Michael A. Zenk
Stanislav Gordeyev
David Cavalieri
University of Notre Dame
Institute for Flow Physics and Control
Notre Dame, Indiana 46556
E-mail: ejumper@nd.edu

Matthew R. Whiteley
MZA Associates Corporation
1360 Technology Court, Suite 200
Dayton, Ohio 45430

Abstract. We provide a background into aero-optics, which is the effect that turbulent flow over and around an aircraft has on a laser projected or received by an optical system. We also discuss the magnitude of detrimental effects which aero-optics has on optical system performance, and the need to measure these effects in flight. The Airborne Aero-Optics Laboratory (AAOL), fulfills this need by providing an airborne laboratory that can capture wavefronts imposed on a laser beam from a morphable optical turret; the aircraft has a Mach number range up to low transonic speeds. We present the AAOL concept as well as a description of its optical components and sensing capabilities and uses. © *2013 Society of Photo-Optical Instrumentation Engineers (SPIE)* [DOI: 10.1117/1.OE.52.7.071408]

Subject terms: aero-optics; adaptive optics; Airborne Aero-Optics Laboratory.

Paper 121413SSP received Sep. 27, 2012; revised manuscript received Jan. 8, 2013; accepted for publication Jan. 9, 2013; published online Feb. 28, 2013.

1 Introduction

In the late 1970s and early 1980s, optical turrets where extensively studied as the use of high-energy lasers on aircraft became feasible. During that period, the Airborne Laser Laboratory (ALL) successfully demonstrated the usefulness of airborne high-energy lasers.[1] The ALL used a carbon dioxide, gas-dynamic laser; but the laser's long wavelength (10.6 μm) limited its range and intensity on target. From a diffraction-limited point of view, the range and intensity of an airborne system can be increased by two orders of magnitude by moving the laser wavelength to 1.0 μm, see Fig. 1(a). In the past two decades, high-energy chemical lasers moved toward the 1.0-μm mark; notably the chemical oxygen iodine laser (COIL) used on the airborne laser (ABL), which lased at 1.315 μm. More recently, high-energy, solid-state lasers are beginning to become a reality with wavelengths right at 1 μm. As solid-state laser technology and adaptive-optic systems continue to improve, the use of lasers for directed energy and communication applications has taken on new life; however, the shorter wavelengths (1 to 1.5 μm) of these new lasers are more affected by the inhomogeneous refractive mediums surrounding the aircraft.[2,3] When the source of the inhomogeneous refractive medium results from turbulence in the flow over and around the turret on an airborne platform, the problem is referred to as "aero-optics,"[2–4] and its presence imposes an opposite effect on range and intensity from that of the diffraction-limited enhancements of the shorter wavelengths, as can be seen in Fig. 1(b).[3,5] For the ALL, aero-optics posed only a 5% reduction in diffraction-limited performance.

Because the aero-optic effects on ALL were only about 5%, by the end of the 1980s, all funding for research in aero-optics had come to an end, and system designers took this as reassurance that overall system impact of aero-optics on airborne-laser performance could always be estimated as being 5% or less, regardless of laser wavelength; on the other hand, the physics, as shown in Fig. 1, said otherwise. The plot in Fig. 1(b) is based on the large-aperture approximation,[6] where the Shrehl ratio, SR, the ratio of actual line-of-sight intensity, I, to the diffraction-limited intensity, I_o, can be approximated as

$$\mathrm{SR} = \frac{I}{I_o} = e^{-\left(2\pi\frac{\mathrm{OPD_{rms}}}{\lambda}\right)^2}, \tag{1}$$

where $\mathrm{OPD_{rms}}$ is the spatial root-mean-square (rms) of the optical path difference, and λ is the laser wavelength. An $\mathrm{OPD_{rms}}$- reducing SR by 5% at 10.6 μm becomes a serious problem when the wavelength is reduced by 10, as can be seen in Fig. 1(b). While the atmosphere is also an inhomogeneous refractive medium, and thus the effect of the atmosphere is also exacerbated by the shorter wavelengths, the spatial and temporal frequencies associated with aero-optics are far higher than those due to the atmosphere, so adaptive-optic mitigation approaches are much more difficult to develop. The consequence of aero-optics for the shorter wavelengths effectively limits the laser-system's field of regard, and yet a large field of regard is essential to making airborne laser systems practical for directed energy and free-space communication.

Driven by the desire to have a large field of regard, from a strictly mechanical point of view, the use of a hemisphere-on-cylinder turret appears to offer the best field of regard as well as a simple, mechanically efficient means to project or receive laser radiation to or from a target; however, the flow around a turret is fairly complex and contains density (thus index-of-refraction) fluctuations and creates aero buffeting.[7] These effects result in beam jitter (line-of-sight error) and, as referred to above, higher-order wavefront aberrations that reduce the peak irradiance of the laser beam in the far-field. Aero-buffet-induced jitter's detrimental influences increase with range. This impairs the capacity of shorter wavelengths to increase the range. One would think the prior research in aero-optics in the 1970s and early 1980s would be directly transferable to the new interest brought by the new shorter-wavelength high-energy lasers, but it is not. Other than being somewhat useful for estimating how large the problem might be, it is of little use because the data survives primarily as statistical estimates of $\mathrm{OPD_{rms}}$ for a few geometry-dependent turret configurations. The

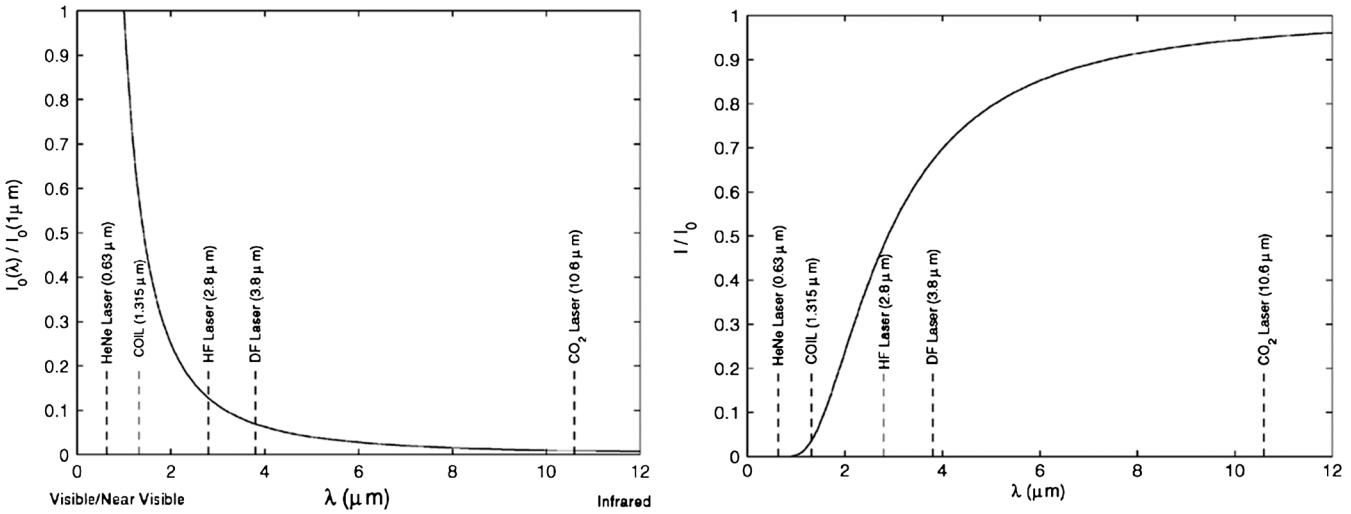

Fig. 1 Opposite effects: (a) peak irradiance of diffraction-limited spot; (b) effect of wavelength on aero-optically aberrated system performance.[3,5] COIL—chemical oxygen iodine laser, HF—hydrogen fluoride, DF—deuterium fluoride.

reason for the paucity and character of the data is due to the tools then available for capturing the aberrations, double-pulsed interferometry and hot-wire measurements of the flow field from which a linking equation was used to infer OPD_{rms}.[3,5,6] Both of these methods relied on assumptions that, in some cases, have now been shown to be incorrect and in other cases left the estimates with large uncertainty. What was completely missing were long time series of time-resolved wavefronts.

A research initiative by AFOSR in the mid-1990s reinstated funding for aero-optics based on the recognition that aero-optics might be important to shorter-wavelength airborne laser systems. Early work under this initiative produced the first truly high-frequency wavefront sensor, the small-aperture beam technique sensor which operated at 100 + kHz, and its serendipitous application to laser propagation through a Mach 0.8 separated shear layer at Arnold engineering development center (AEDC).[8,9] The AEDC wavefront measurements demonstrated two important facts; the first was that the aero-optic problem was much larger than had been presumed, and second, the cause of the aberrations was not understood. These facts led to continued support for aero-optics research that eventually led to a rational basis for the cause of the aberrations,[10] and also documented aero-optical effects on various-geometry turrets of interest and research into mitigating the effects through flow-control approaches, adaptive-optic approaches, combinations of these, as well as interest in being able to predict these effects using computational fluid dynamics. Still, until only a few years ago, all of the experimental work was performed in wind tunnels. The increased interest in aero-optics also led to continuous improvements in wavefront sensing capabilities and instrumentation.

Almost exactly five years ago, in 2007, the High-Energy Laser, Joint Technology Office (HEL JTO) recognized the need to evolve the study of aero-optics to in-flight research and thus was created the Airborne Aero-Optics Laboratory (AAOL) program. Now in its fifth year, starting as a concept and through a close working relationship led by the University of Notre Dame with Boeing SVS, the Air Force Institute of Technology, MZA Associates, and Northern Air, the AAOL program is now producing time-resolved time series of wavefronts that have proliferated through the government, industry, and university communities, and have become the mainstay of research in understanding and mitigating aero-optic effects. Further, line-of-sight jitter data obtained from the program have been identified as the bench-mark data for developing jitter prediction and mitigation techniques for future airborne laser programs. This paper describes the AAOL program from concept to realization, and, in as much as possible, describes the experimental set up of the source and laboratory aircraft, for much of the data that is presently being cited in the literature. To this end, the paper begins by describing the AAOL concept and then its implementation. Also included is a description of the evolution of wavefront sensor instrumentation used on the laboratory aircraft. Other than giving a brief exposure to the type wavefront data collected, this paper defers to the detailed description of data and the treatment of that data to other papers (see, for examples, Refs. 11–14).

2 AAOL Concept

The ultimate objective of the AAOL program is to obtain in-flight data about the effect that the various types of turbulence over and around a turret have on wavefronts for a laser beam propagated from the turret; because the effect is reciprocal, this information can be determined by receiving rather than projecting a beam. The reciprocal characteristic is, in fact, the basis for adaptive optics.[15] Still, the problem of creating an appropriate incoming beam is not a trivial one. In adaptive optics, determination of the wavefront which must be corrected for is measured from an incoming beam, but the source of this beam is from a distant beacon that may be available from a glint off the distant target or the creation of a guide star. In the case of free-space communication, using lasers as the source of the beam can be a laser projected from a cooperative target. If the source of the incoming beam is from a distant target or guide star, the incoming beam is already imprinted with aberrations due to its traverse through the atmosphere. In order to avoid, and thus simplify the

interpretation of wavefronts obtained through a turret on the laboratory aircraft, the AAOL program proposed using a beam from a source aircraft flying in relatively close formation to the laboratory aircraft. But, this posed a further dilemma of generating a "pristine" beam that arrives at the laboratory aircraft's turret pupil without having been corrupted by aero-optical effects from the flow around the source aircraft.

The concept finally proposed was to have the source beam leave as a small diverging beam, originating from the source aircraft with a beam diameter of only a few millimeters, and then diverging to overfill the pupil aperture on the laboratory aircraft turret by two times. The proposed formation flight distance from exiting source beam to the laboratory's turret pupil was 50 m. The rational for the use of the small beam at the source was that the beam would be small compared to the coherence length of the optically relevant turbulent structures inside a thin turbulent boundary layer present on the skin of the laser aircraft[16]; the beam's small diameter would then only allow the boundary-layer turbulence on the source aircraft to impose slight tip-tilt on the beam. By the time the beam propagated 50 m, the wavefront on the beam would nominally be spherical so that any tip-tilt on the beam at the source would not affect the spherical figure on the arriving beam at the laboratory aircraft. In the first year of the program, extensive analysis of this concept was performed using WaveTrain, a wave-propagation code that also is able to simulate components of optical beam trains and instrumentation. More details on WaveTrain can be found in Ref. 17. These analyses demonstrated the concept was indeed valid, and the main effect of uncertainties introduced into wavefront measurements was associated with the nonuniform intensity profile of the source laser beam and focus errors for the telescope relative to the distance between the emerging source beam and the laboratory aircraft's turret pupil, and pointing errors of the source laser, which offset the beam from the turret's center.

In analyzing the nonuniform intensity in the source beam, it was found that its main effect was to cause a very slight tracking error in the laboratory turret's track algorithm, and this could be minimized by optimizing the source beam's divergence angle, which, in turn, was governed by the distance between aircraft so that the diverging beam overfilled the laboratory turret's pupil aperture by two times. As it turned out, the proposed 50 m was almost exactly the optimum distance, so the distance was kept at the proposed 50 m. These conclusions may be inferred from the plots given in Figs. 2 and 3. Figure 2(a) shows the effect of divergence angle for a 50-m separation on pointing error with a Gaussian intensity profile and a 1-in. obscuration, D_{obs}, caused by the telescope secondary mirror; it is clear that a divergence angle of 4.92 mrad minimizes the tracking error for a turret with small focus error. Figure 2(b) is an expanded plot for just the 4.92 mrad case; the inset figures show the effect at the focal plane for a well-focused beam, top, and ghosting effect of an out-of-focus beam (bottom). At a range of 50 m, the divergence angle to overfill the full aperture (12.25 cm) turns out to be 4.92 mrad (the clear aperture is 10 cm).

The centroid focus error in Fig. 2, as shown in the bracketed curves, was based on the acceptable tolerance on knowing the range between the source beam and the turret pupil to yield a measure of wavefront error better than $\lambda/20$ for a laser wavelength of 532 nm and a 10-cm clear aperture pupil. Figure 3(a) shows that for a separation distance of 50 m, the range must be known to ± 5 cm. Figure 3 shows the coupled effect on the fractional power in the beam as it arrives on the optical bench as a function of pointing error; this curve was used to set the power requirements in the source laser depending on the selection of instruments being used in the laboratory aircraft.

The selection of 50 m was primarily driven by the desire to not have atmospheric turbulence corrupt the aero-optical data. This too was analyzed and an example from that analysis is shown in Fig. 4. Figure 4 shows the measured wavefront error at a viewing angle of 130 deg based on aero-optic data obtained in wind-tunnel experiments. Viewing angle is a way of combining azimuth and elevation[7]; a viewing angle of 130 deg indicates that the pupil is directed aft. The top row of figures show the laser illumination at the turret pupil prior to traversing the aero-optical turbulence, the phase map of the

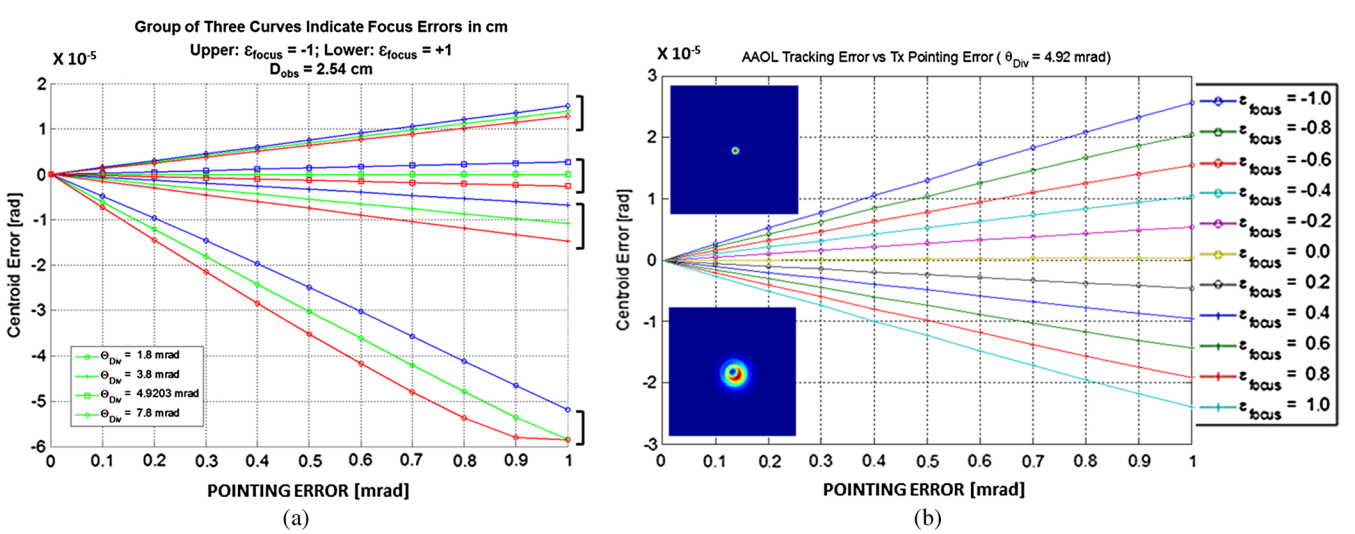

Fig. 2 (a) Tracking errors with central obscuration, $D_{obs} = 2.54$ cm, for various divergence angles, Θ_{DIV}; (b) expanded portion of left curve showing only the case for divergence angle, $\Theta_{DIV} = 4.92$ mrad; AAOL = Airborne Aero-Optics Laboratory.

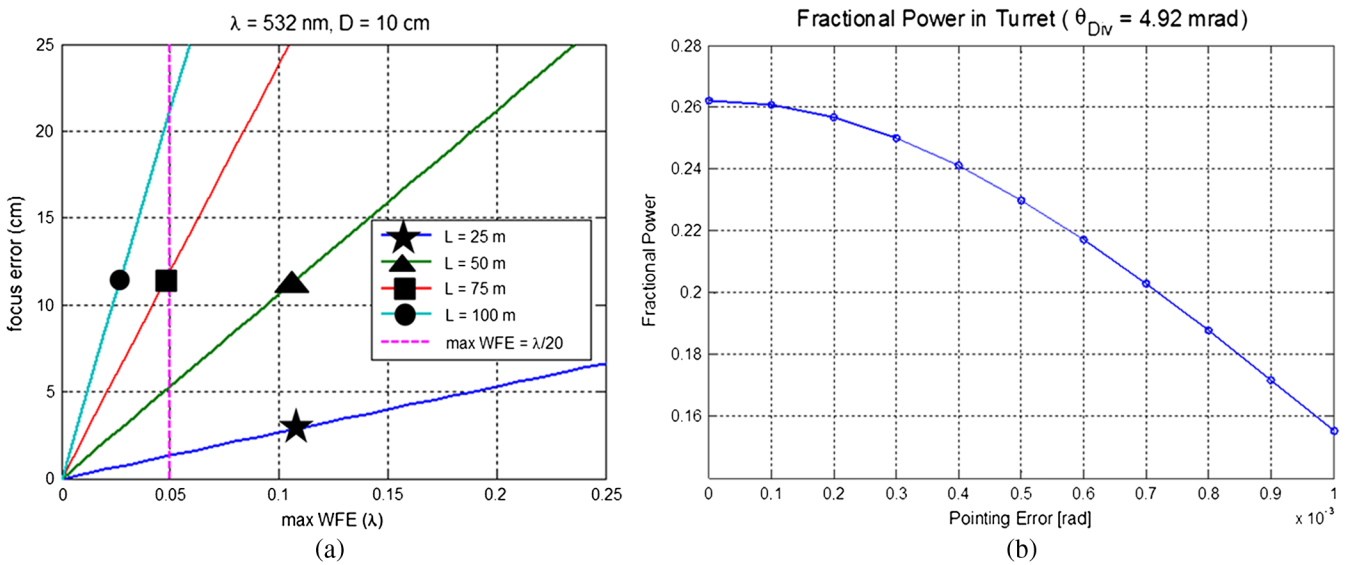

Fig. 3 (a) Effect of error in distance measurement on maximum wavefront error (WFE) measured for $\lambda = 532$ nm and the AAOL aperture diameter (10 cm); (b) effect on beam power on power in the beam as it arrives onto the optical bench including the coupled effect of laser pointing and turret focus error.

beam with the aero-optical distortion imposed at the pupil location, the phase map only at the pupil and the far-field pattern because of the aero-optical only wavefront error. The lower row is the same sequence of results with an exaggeratedly large free-stream, atmospheric turbulence condition with r_o equal to 5 cm, representing turbulence strength, C_n^2, three orders of magnitude larger than would be reasonably expected to be encountered at the AAOL flight altitudes. The results shown in Fig. 4 are representative of a large number of realizations used to gather sufficient statistics to conclude the effect of the atmosphere with the proposed concept could be ignored for the 50 m propagation distance.

The analysis discussed above demonstrated the basic concept was valid, but it was also useful in setting additional requirements on the AAOL system. One of the objectives of the aero-optical measurements was also to be able to measure the stationary portion of the aberration due to the mean density "lens" imposed by the variation in the air's density due to its deceleration and acceleration over the turret as the incoming flow stagnates in the front of the turret than accelerates over it; this component of aberration is referred to as

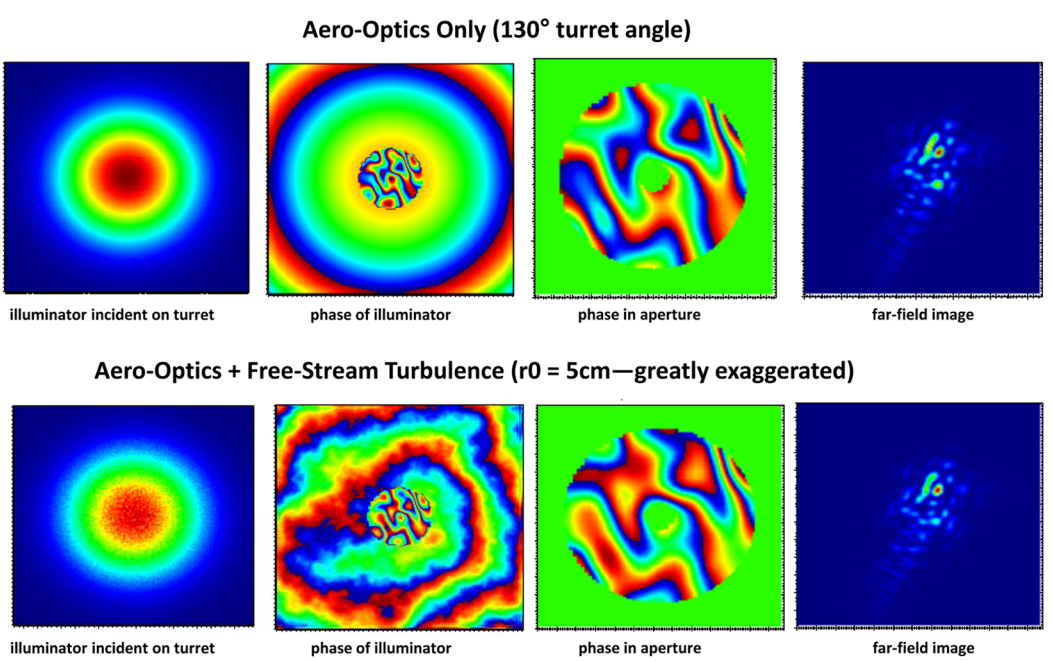

Fig. 4 Example of the effect of on the measurement of aero-optical wavefront error in the presence of strong atmospheric turbulence ($r_o = 5$ cm) and in the absence of any atmospheric turbulence for a 50-m separation between the diverging source beam and the turret pupil in the laboratory aircraft.)

aero-dynamic lensing. In theory this should be obtainable by the mean aberration over the time series from a fixed viewing angle; however, recall that the arriving beam has a spherical figure because of the diverging source beam. Because the aerodynamic lensing itself has a large component of spherical aberration, it is important to separate the diverging-beam curvature from the measurement; in order to do this, the concept included removing the incoming, diverging-beam curvature by mechanically adjusting the turret's telescope prescription to remove the curvature imposed by a nominal 50-m radius. This component resided in the beam train ahead of the fine-track mirror and served the additional purpose of assuring good focus on the position-sensing device that controls the fine-track mirror. When the distance is different from the 50-m compensated wave front, concave or convex spherical curvature is introduced in the beam. It is this defocus which is used in Figs. 2 and 3, discussed earlier. This residual curvature can be removed either mechanically as above, or it can be removed in postprocessing, but in either case, the distance between source and pupil must be known to within ± 5 cm, for both the reasons described earlier, and to further reduce the measured aero-optic wavefronts to less than 0.02 microns, peak to valley, over the full clear aperture. This requirement was originally proposed to be met by using a laser ranging device; however, actual flight environments eventually drove us to using differential GPS, which is accurate to within less than 5 cm. Because of the practical limitations associated with formation flying, being able to know and record the distance between source and turret pupil is used both for instructions to the pilots and in postprocessing data. Error in the separation distance from the nominal 50 m also has some other system implications. One of these is the fact that, because the beam is diverging, it affects the intensity of the arriving beam as it is delivered to the laboratory optical bench and split to the various instruments making use of the beam; however, this problem is relatively easy to account for by allowing for this intensity variation in setting the dynamic range of the sensors. Other than the tracking errors referred to above, defocus also causes the fine-track mirror to be slightly away from the nominal reimage point of the turret pupil; this, in turn, means that when the instruments reimage the fine-track mirror, some beam wander can be present. This slight beam wander is treated in postprocessing, but it is important that data users are aware that this can be present in the raw data and should be removed prior to further analysis. From a practical point of view, it should be noted that another nicety of using a beam from a chase aircraft is that there is plenty of laser energy for a robust tracking system and any number of instruments on the optical bench; however, in taking the wavefront data, one would like to take advantage of the full intensity range of the sensor with the caveats associated with setting the dynamic range. In general, this means adjusting the intensity of the beam using a series of neutral-density filters before it arrives at the sensors in order not to saturate their measurements. It should also be noted that focus error due to errors in the nominal 50-m separation distance also result in variations in the focused wavefront-sensor lenslet beams, but this seldom causes sufficient problems to make a particular wavefront time series unusable. Before finally working out the problems with various approaches to obtaining the distance, some early AAOL data had issues with saturation caused primarily by the aircraft being too close. Since settling on the use of differential GPS, these problems have gone away.

By the end of the first year of the program the concept was fully validated and the requirements for both optical systems in the source and laboratory aircraft set. The final decision which had to be made was the selection of the aircraft to be used for the program. This selection was based on criteria developed from aero-optic testing in wind tunnels. These criteria imposed Mach number requirements on the choice of aircraft. These Mach number limits were derived from Reynolds number considerations. Based on turret diameter, D, the Reynolds number is given by

$$\mathrm{Re}_D = \frac{\rho U_\infty}{\mu}, \tag{2}$$

where ρ is the air density at altitude, μ is the viscosity, and U_∞ is the incoming free-stream air speed. Wind-tunnel testing had shown that if a one-foot diameter turret was used, the minimum flight speed had to be at least Mach 0.4 in order for the collected data to be scalable to larger turrets and other altitudes for flight Mach numbers up to 0.55; the minimum Reynolds number based on diameter should be greater than 0.5×10^6. Figure 5 shows a plot of Reynolds number versus flight Mach number at various altitudes for the AAOL turret diameter.

The Mach 0.55 limit to scaling wavefront data resulted from the known fact that at Mach numbers above 0.55, the flow over the turret will attain sonic conditions; that is to say, for flight Mach numbers above 0.55, the flow over the turret will contain regions of both subsonic and supersonic flow, making the flow over the turret transonic. In order to collect data in the transonic regime and have at least enough margin to establish scaling laws, the flight Mach number had to reach at least Mach 0.7. The other constraint on the choice of aircraft was based on cost. The AAOL concept was to limit the cost by making use of commercially available business jets so the overall cost of flying the aircraft would be shared with other uses of the aircraft by switching the aircraft in and out of experimental status. After seeking cost estimates from several business jet providers that were willing to take their aircraft in and out of passenger status, Cessna Citations were chosen as the

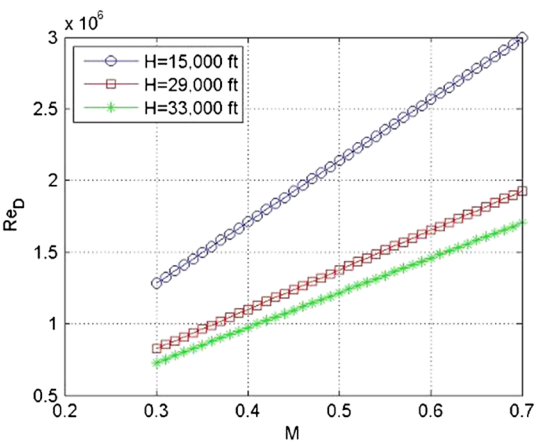

Fig. 5 Reynolds number versus flight Mach number for a 12-in. (30.48 cm) diameter turret at various altitudes. M—Mach number; Re$_D$ReD—Reynolds number based on turret diameter.

airborne platforms for the AAOL program. It should be noted that all modifications we made to the aircraft for use in data campaigns required FAA certification to both place the aircraft into experimental status and return them to passenger status.

3 Aircraft Flight Operations and Overall Description

Based on the discussion of the overall concept, requirements, and constraints, the AAOL flight program consists of two Cessna Citation Bravo aircrafts flying in formation at a nominal separation distance of 50 m. A diverging, small-diameter, CW YAG-Nd laser beam is sent from a chase plane to an airborne laboratory, see Fig. 6. The turret on the laboratory aircraft consists of a 12-in. diameter (30.5 cm) turret with a 4-in. (10.16 cm) clear-aperture; the window can be either flat or conforming to the spherical figure of the turret (i.e., conformal). The turret itself presents a mold line that is a hemisphere on a cylindrical base, when installed in the aircraft, protrudes out the side of the Citation through a modified escape hatch. The cylindrical base has cutouts at opposing 180-deg positions so that the turret pupil is not obscured at elevation angles of 0 deg it should also be pointed out that two approximately 2-mm gaps/slits are present in the turret mold line between the main, elevation portion of the turret gimbal and the supporting trunnions. The turret can be extended so that the cylindrical base protrudes into the airstream by a nominal 4 in. (10.16 cm), or withdrawn so only the hemisphere protrudes into the airstream. At 50 m, the beam from the chase aircraft diverges to approximately 20 cm so that it overfills the turret aperture by a factor of two; as discussed in Sec. 2, the diverged beam presents a nominal spherical wavefront at the laboratory-aircraft turret pupil, passing through the aero-optical disturbance and is captured into the turret's beam train. Once the laser and turret systems are tracking each other, a 2.0-cm, stabilized beam emerges from the turret mounting "box" onto the optical bench in the laboratory aircraft, nominally with the spherical figure due to the divergence from the chase aircraft removed; however, if the separation distance is greater or less than 50 m, some residual curvature will remain. The "stabilization" of the beam is performed by a closed-loop, fast-steering mirror system which nominally reimages the turret pupil and reduces the beam's overall jitter to a cut-off frequency of approximately 200 Hz, thus acting as a high-pass jitter filter (also refer to the comments regarding beam stabilization in Sec. 2). The "stabilized beam" is then split between the various sensors on the optical bench onboard the laboratory aircraft. Details of the experimental set-up will be discussed later in this paper.

(a) (b)

Fig. 6 Airborne Aero-Optics Laboratory (left) schematic of the two citations flying in formation; (right) picture taken during a flight test, note laser on the turret.

As mentioned above, the only modification to the external portion of the laboratory aircraft is the replacement of the emergency escape hatch located just aft of the cockpit right seat. For this purpose, a spare escape hatch was purchased and modified by replacing the structural components and skin of the central portion of the hatch with a solid machined piece of aluminum through which the turret hole was located as well as needed pressurization interface components that mated with portions of the turret assembly on the interior of the aircraft. In addition to the main turret hole, there are also two holes/ports below the turret that can be filled with either instrumentation devices or plugs, as shown in Fig. 7(c). These ports have been used for boundary-layer measurement devices and other type measurements and experiments; one insert for measuring the incoming boundary layer profile is shown in Fig. 7(c). Two other devices are worth mentioning, one of these has a small optical window at the center and a support bridge holding a first-surface mirror; this insert is used for making in-flight, attached turbulent-boundary-layer wavefront measurements,[16] and is shown in Fig. 7(d). A second insert accommodates a larger, high-optical quality window for supporting lidar and other experiments. Figure 7(a) is also useful in pointing out the two small apertures on the turret above the main telescope aperture; these are flush with the spherical contour of the turret, but are flat.

4 Laboratory Turret Assembly and Source Aircraft Laser and Tracking System

To prepare the laboratory aircraft for flight, all of the seats except the two aft-most passenger seats are removed from the aircraft along with portions of the interior padding. Then a 1.2- cm thick, 0.6×3-m aluminum plate is firmly mounted to the seat rails on the starboard side of the aircraft. The turret assembly is mounted on a 0.61×3.05-m optical bench, and the bench then mounted to the aluminum plate. The turret assembly consists of a hefty aluminum box-like structure

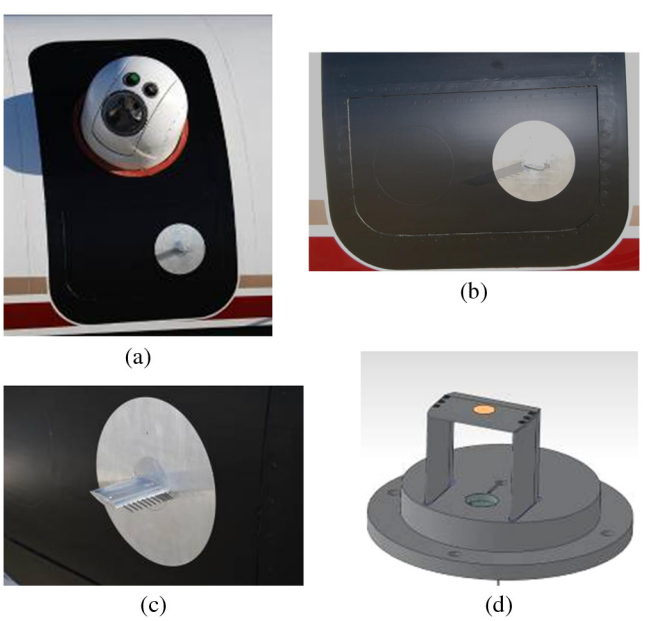

(a) (b) (c) (d)

Fig. 7 Modified escape hatch (a); close up of lower portion of hatch showing a boundary layer probe insert (b) and (c); and boundary-layer optical insert (d).

onto/into which the gimbaling turret structure containing the telescope Coude path, gear mechanism, course- and intermediate-track cameras and pressure collar are mounted. A rubber boot completes the pressure seal. Inside the box, a small percent of the beam's intensity coming from the Coude path is split to a fine-track mirror's position-sensing device. The electrical connections to the turret azimuth and elevation gear motors as well as the acquire-and-track cameras are fed into the box through the cable wrap and eventually out of the box structure to a tracking processor along with the fine-track signals. Once the turret system has acquired the incoming beam from the source aircraft, the turret automatically holds track. The overall arrangement of the turret assembly is shown in Fig. 8. The last element in the beam path inside the box is the fast-steering mirror that holds fine track; just before being spit to the fine-track mirror's position-sensing device, the nominal spherical aberrations from the diverging beam are removed.

As previously mentioned, the fine-steering mirror is located at the nominal pupil reimage location (see comments in Sec. 2). From the fine-track mirror, the beam emerges from the box onto the optical bench as a 2-cm beam, nominally stabilized up to 200 Hz. Once delivered to the bench the beam is split into the various instruments used for the various experiments being flown. At least two instruments are always present on the bench; the first is a jitter-recording device consisting of focusing optics and a position-sensing device which records the residual jitter remaining on the beam after the fine-track mirror at data rates up to 200 kHz, although the usual practice is to gather these data at ~100 kHz. The second instrument is a high-bandwidth wavefront sensor, versions of which are described later in this paper. The layout with these two instruments in place on the bench in the aircraft is shown in Fig. 9.

The source laser system in the second aircraft is a relatively simple installation and requires only two of the seats on the port side of the aircraft be removed. The laser power supply is attached directly to the seat rails and receives its laboratory power from similar, permanently installed inverters as that in the laboratory aircraft. The differential GPS is attached to one of the passenger windows at the same location aft of the laser as the GPS system is aft of the turret in the laboratory aircraft. The laser pointing and tracking system is then attached through a separate constructed bracket system that serves as the optical bench for the laser head and the heliostat tracking system. A schematic and two photographs of the system are shown in Fig. 10. Other than the inverters, the only other permanent modification to the aircraft was the purchase of a new window through which the beam emerges from the aircraft. While there is no real control on what happens to the window, the inner protective transparent liner of the window that is normally installed in the aircraft is removed during testing, and the maintenance crew is instructed to use care and special cloths in cleaning that particular window.

5 Evolution of Wavefront Sensors Used in the AAOL Program

At the time the AAOL was first proposed, the availability of high-frame-rate wavefront sensors was far more limited than it was when the first data-acquisition flight occurred. The overall objectives of the program were to gather high-temporal and high-spatial resolution time-resolved wavefront time series. Earlier experience with curvature sensors that depend on intensity differences ahead of and behind the nominal focal plane of an imaging camera indicated that while these type sensors could theoretically provide both the spatial and temporal resolution desired, real-environment

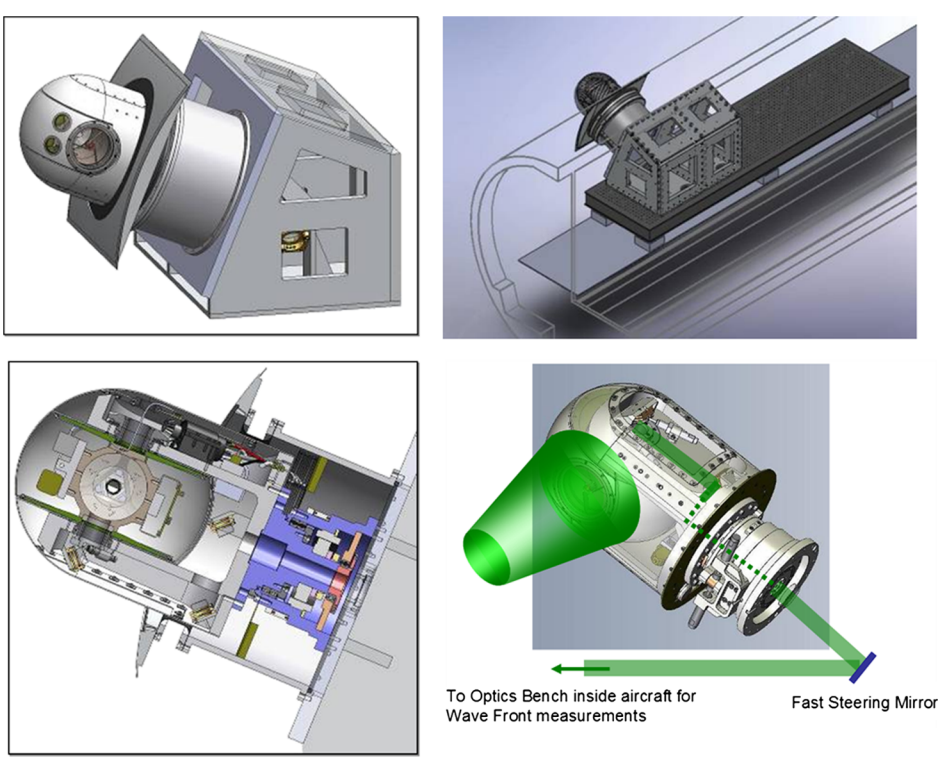

Fig. 8 Optical turret assembly schematic.

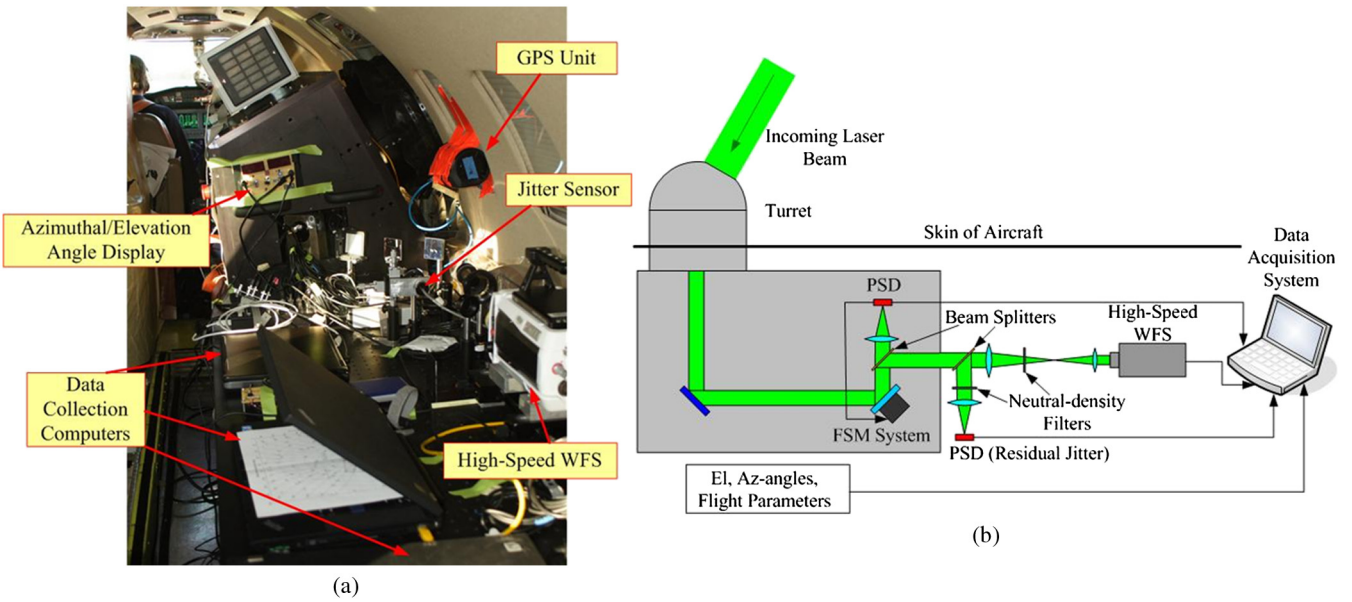

Fig. 9 Photograph of turret assembly on the optical bench inside the aircraft (a) and beam-train schematic (b). PSD—position sensing device, FSM—fast steering mirror, WFS—wavefront sensor, GPS—global positioning system.

effects like vibration and line-of-sight jitter made this type sensor impractical to use; in every case in which it was used, it required extensive analysis to retrieve good-quality wavefronts and often failed to recover any usable data. Our experience further led us to conclude that Shack-Hartmann sensors provided the most-robust and reliable wavefront sensors that could provide reliably good data from flight experiments. At the time of the original proposal, truly high-bandwidth video cameras were still in their formative stages and the on-camera memory was limited to too-few frames to provide long time-series of data, and they required arduous and time-consuming procedures to remove the camera-stored data from the on-camera ram.

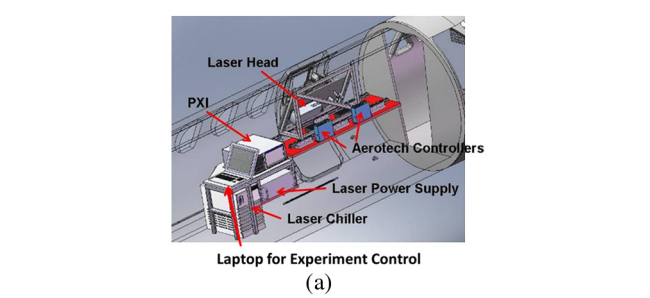

Fig. 10 Schematic of general placement of the laser tracking system and beam train in source aircraft (a); photograph of the system being tested in the laboratory (b); and system mounted in aircraft (c).

This being the case, we developed a hybrid analog-digital 10×10-subaperture, Hartmann-type sensor that allowed us to record wavefront slopes at 125 kHz for long periods of time and the data was read to disk in near real time; this sensor also has a real-time capability.[18] Although the sensor had high temporal rates, the spatial resolution was limited. To record the smaller aberration structures that might be missing, we proposed recording simultaneous, but much lower frame-rate 33×33-subaperture wavefronts on a Wavefront Sciences CLAS-2D sensor that framed at up to 30 Hz. Use of the combined sensors in wind-tunnel experiments gave relatively good results for inferring both the spatial and temporal character of the aero-optic wavefronts; however, before the first data-acquisition flight, we experimented with mating an AOA lenslet array with a newly purchased high-frame-rate video camera that the University of Notre Dame acquired for other research. Our first use of the newly assembled Hartmann sensor gave amazingly good results which were bench-marked against the CLAS-2D sensor and gave essentially identical results when recording static aberrations. Although new in-house developed software is now routinely used to reduce wavefront data, we initially made use of the Wavefront Sciences software, by permission.

The first system assembled made use of a Photron FastCam SA1 camera which could frame at up to 20 kHz for a 32×32-lenslet array sensor and collect reasonably long time series of wavefronts, also adjustable shutter speeds down to a few microseconds were possible, and were sufficient to essentially freeze the wavefronts, but the download times of the camera data onto a disk were between 15 and 20 min per collection. The next advance in our wavefront sensing was to move to a Vision Research high-speed Phantom V710 camera, which had flash memory on-board that could be downloaded from the camera in less than a minute; this greatly increased the productivity of every flight. Finally that camera was replaced with Vision Research's Phantom V711, which has an even quicker data download capability and frames at up to 25 kHz for the 32×32-lenslet

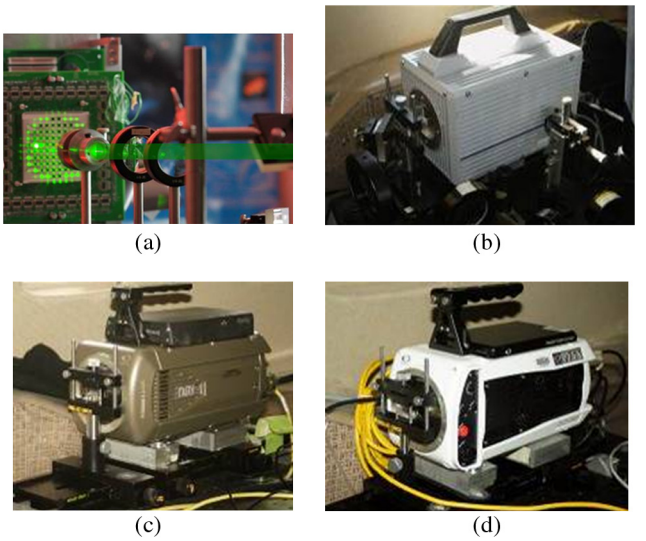

Fig. 11 Four of the high frame-rate wavefront sensors used in AAOL program: (a) in-house developed 10×10 analog-digital wavefront sensor—100 + kHz; (b) High-Speed Photron FastCam-SA1 camera, sampling rate—20 kHz; (c) High Speed Phantom v710 camera from Vision Research with on-board flash-memory, sampling rate—20 kHz; (d) High Speed Phantom v711 camera from Vision Research with on-board flash-memory, sampling rate—25 kHz.

array with shutter speeds down to 0.3 ms. If more spatial resolution is desired, the integration area on the camera's image sensor, i.e., charge coupled device array, can be increased to accommodate a 64×64-lenslet array with a reduction in frame rate to 7 kHz; while this is not a sufficient rate to obtain time-resolved successive frames, it is useful in verifying that we are not missing spatial resolution. Four of the high frame-rate wavefront sensors described here are shown in Fig. 11.

6 Data Types Collected on AAOL

As mention previously, the data routinely collected on the AAOL consists of residual beam jitter and high-bandwidth wavefront time series. Although the jitter data is self-explanatory, it is worth mentioning that extensive data of this kind accompanied by wavefront and fine-track mirror data is somewhat unique. From time to time, these jitter measurements have been recorded along with several accelerometers placed at strategic locations on the turret assembly. These data can be used as benchmark data for aero-buffet studies in conjunction with detailed finite-element modeling of the full turret and optical system.

The wavefront data that presently exist cover a wide range of Mach numbers and altitudes. These Mach numbers range from Mach 0.4 at 15 kft to Mach 0.69 at 36 kft. But also, the wavefront data include acquisitions for the various morphable configurations of the turret. As suggested earlier, these configurations include a flat or conformal window over the aperture, and either the cylindrical base protruding into the airstream by a nominal 10 cm, or having only the hemispherical portion of the turret protrude into the airstream. In the future, the turret will be further modified with flow-control devices attempting to mitigate the aero-optic effects to open up the field of regard.

Based on dealing with wavefront data for more than a decade, certain scaling laws allow the data we collect to be scaled to different Mach numbers, altitudes, and turret diameters as long as the minimum Reynolds-number threshold has been met. In addition to experience in collapsing experimental data there are theoretical reasons for these scaling laws that involve known fluid-mechanic scaling arguments, the rationale for which is discussed in Ref. 7; however, for the purposes of this paper, we want to make use of these scaling laws to demonstrate the productivity of the AAOL program.

The data scaling falls into two parts that deal with wavefront error amplitude scaling and aberration convection speeds which adjust the frequency of the wavefront capture rate. For amplitude scaling we nondimensionalize the OPD by Eq. (3). For the AAOL, the aperture is 1/3 the turret diameter so that as long as this ratio is retained, the OPD can be for any altitude, Mach number, and turret diameter by simply multiplying by the new parameters. We know this works well as long as the flow over the turret is fully subsonic. Although we have not determined if this scaling extends into the transonic range, the same nondimensionalization is applied to the data. At least for the fully subsonic case, this scaling of OPD works equally well for amplitude scale of individual frames of wavefronts as well as $\mathrm{OPD}_{\mathrm{rms}}$ of a wavefronts over their aperture.

The nondimensional OPD expressed as $\mathrm{OPD}_{\mathrm{Norm}}$ is usually given in units of microns per meter so that

$$\mathrm{OPD}_{\mathrm{Norm}}\left(\frac{\mu\mathrm{m}}{m}\right) = \frac{\mathrm{OPD}}{\left(\frac{\rho_0}{\rho_{\mathrm{SL}}}\right) M^2 D}. \tag{3}$$

The spatial distribution of the aberrations is also normalized by the aperture, which allows rescaling to any aperture diameter with the same aperture to diameter ratio, by simply rescaling to the new turret by using the turret diameter. Rescaling of the framing rate of the wavefront sensor, f, makes use of the Strouhal number, St_D

$$\mathrm{St}_D = \frac{fD}{U_\infty}, \tag{4}$$

meaning our data is presented in nondimensional form. The viewing angle, α, mentioned in Sec. 2, is also helpful in organizing data; as mentioned earlier, it combines turret azimuth and elevation into a single angle.

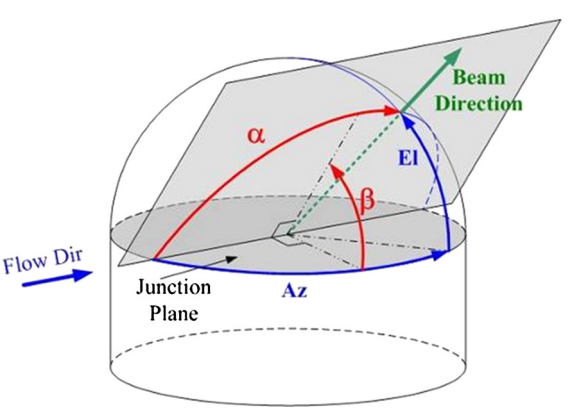

Fig. 12 Relationship between viewing angle (α), modified elevation angle (β), azimuth (Az), and elevation (El) angles.[7]

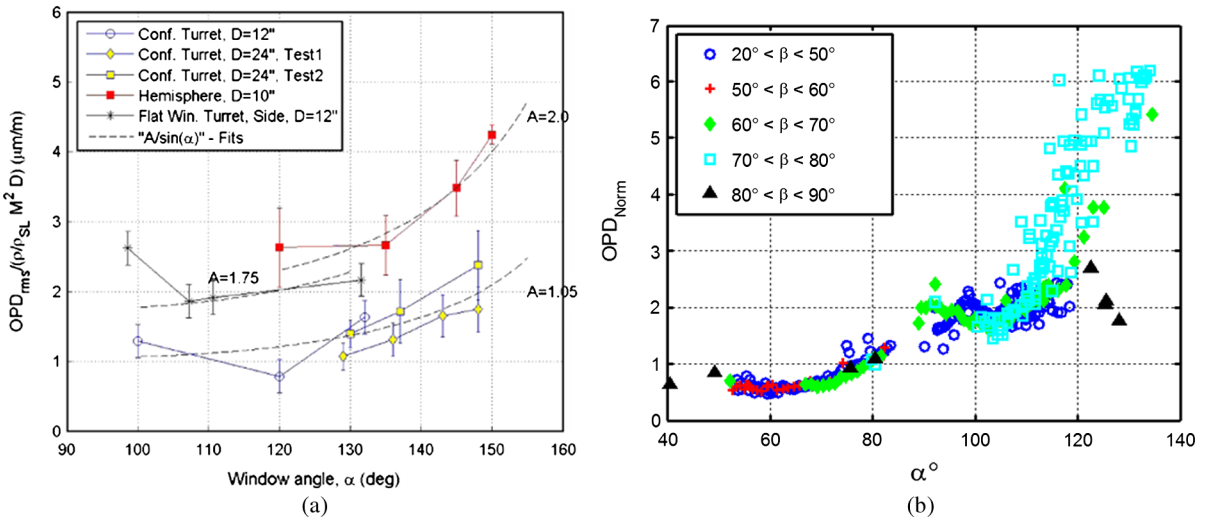

Fig. 13 (a) Available data as of January 2010[7]; (b) data from a single flight sequence.[19] D = diameter.

Referring to Fig. 12, the relationship between the viewing angle and azimuth, Az, and elevation, El, is given by

$$\alpha = \cos^{-1}[\cos(\mathrm{Az})\cos(\mathrm{El})]. \tag{5}$$

The modified elevation angle, β, which is used to account for elevation-specific effects, is given by

$$\beta = \tan^{-1}\left[\frac{\tan(\mathrm{El})}{\sin(\mathrm{Az})}\right]. \tag{6}$$

Again, the nondimensionalized $\mathrm{OPD}_{\mathrm{Norm}}$ and viewing angle, α, are commonly used to present AAOL data. In order to demonstrate the productivity of the AAOL, consider Fig. 13(a), which shows a fair representation of the amount of aero-optical data available in January of 2010[7]; the data shown in Fig. 13(b) came from two flights lasting approximately 2 h each.[19] To be sure, the data in Fig. 13(a) represents a large amount of wind tunnel data synthesized into a single figure, and contains data from different turret configurations; however, the angle increments are real and represent the limitations on viewing angles by obstructions in the tunnel structure and the fact that each angle has to be set up separately, which often involves difficult alignment operations.

7 Conclusions

This paper describes the AAOL and treatment of data derived from in-flight experiments so data users in the future are aware of the various complications present in the data, and the effect of complications on final data products. Enough scaling information was also included so that use of the data in whatever form, including long time series of normalized wavefronts, can be properly scaled to whatever the specific use of the data is. In Sec. 6, we attempted to convey the productivity of gathering these in-flight data, but, there is still a point that should be made. The comparisons in Fig. 13 give some sense of the relative ease of making AAOL measurements as opposed to wind-tunnel measurements; however, it is clear that using a wind tunnel gives far more flexibility to what is trying to be done. Placement of flow control devices such as extensive suction, for example, might be modeled in a wind tunnel by simply using turret mold lines without requiring all of the complexity contained in a real turret, such as the one used on AAOL. But then the experimenter is faced with the difficulties of making the aero-optical measurements posed by the wind-tunnel environment. There is clearly a need for wind-tunnel testing and the AAOL program contains a wind-tunnel component. Not the least of the tunnel requirements are checking out equipment, turret configurations and modifications, flow-control mitigation devices, and even tracking algorithms before they are flown on the airplane. The actual flight hours are not that expensive, but the setup time and collection of both the flight-test experimentalists and flight crew requires coordination and extensive planning and travel to the operation site that is wasted if, once in the air, an issue is discovered that could have been eliminated through wind-tunnel testing. But once in the air, and everything is working, flight data are far easier to collect than wind-tunnel data. For one, the vibration environment is far better in the air than at a wind tunnel site. Aberrations present on wind-tunnel data resulting from the tunnel environment itself, rather than from the aero-optical phenomena, must be carefully handled, and tunnel aberrations should be removed if possible. There is also the issue mentioned earlier regarding the limited optical access present for every tunnel, even those with the best optical access.

Finally, testing in tunnels which have very high subsonic and low supersonic flow capabilities pose all sorts of difficulties. The pressure vessels that enclose the transonic test sections pose extraordinary optical-access problems. Even when optical access is found, it has restricted angle flexibility and the high-speed flow over the access windows itself is optically active. Finally, the use of these tunnels is usually costly, not to mention the size restriction found in some of the facilities. From our perspective, at least for the high-subsonic Mach number regime, it is far easier and less costly to test in the AAOL or a system like it.

Acknowledgments

These efforts were funded by the High Energy Laser-Joint Technology Office (HEL-JTO) and administered through the Air Force Office for Scientific Research (AFOSR) under Grant No. FA9550-07-1-0574. The U.S. Government is

References

1. R. W. Duffner, *Airborne Laser: Bullets of Light*, Basic Books, Plenum Publishers, New York (1997).
2. K. J. Gilbert and L. J. Otten, Eds., "Aero-optical phenomena," *Progress inAstronautics and Aeronautics series*, Vol. 80, AIAA, NewYork (1982).
3. E. J. Jumper and E. J. Fitzgerald, "Recent advances in aero-optics," *Prog. Aerospace Sci.* **37**(3), 299–239 (2001).
4. M. Wang, A. Mani, and S. Gordeyev, "Physics and computation of aero-optics," *Ann. Rev. Fluid Mech.* **44**(1), 299–321 (2012).
5. K. G. Gilbert, "The challenge of high brightness laser systems: a photon odyssey," *Opt. Eng.* **52**(7), 0091–3286 (2013).
6. V. N. Mahajan, "Strehl ratio for primary aberration in terms of their aberration variance," *J. Opt. Soc. Am.* **73**(6), 860–861 (1983).
7. S. Gordeyev and E. Jumper, "Fluid dynamics and aero-optics of turrets," *Prog. Aerospace Sci.* **46**(8), 388–400 (2010).
8. R. J. Hugo et al., "Time-resolved wave front measurements through a compressible free shear layer," *AIAA J.* **35**(4), 671–677 (1997).
9. E. J. Fitzgerald and E. J. Jumper, "Aperture effects on the aerooptical distortions produced by a compressible shear layer," *AIAA J.* **40**(2), 267–265 (2002).
10. E. J. Fitzgerald and E. J. Jumper, "The optical distortion mechanism in a nearly incompressible free shear layer," *J. Fluid Mech.* **512**, 153–189 (2004).
11. N. De Lucca, S. Gordeyev, and E. Jumper, "In-flight aero-optics of turrets," *Opt. Eng.* **52**(07), 071404 (2012).
12. D. J. Goorskey, R. Drye, and M. R. Whiteley, "Spatial and temporal characterization of AAOL flight test data," *Proc. SPIE* **8395**, 839509 (2012).
13. S. Abado, S. Gordeyev, and E. Jumper, "Approach for two-dimensional velocity mapping," *Opt. Eng.* **52**(07), 071402 (2012).
14. M. R. Whiteley, D. J. Goorskey, and R. Drye, "Aero-optical jitter estimation using higher-order wavefronts," *Opt. Eng.* **52**(7), 071411 (2012).
15. R. K. Tyson, *Principles of Adaptive Optics*, 2nd Ed., Academic Press, Boston (1998).
16. A. E. Smith, S. Gordeyev, and E. J. Jumper, "Recent measurements of aero-optical effects caused by subsonic boundary layers," *Opt. Eng.* **52**(07), 071404 (2012).
17. J. D. Mansell et al., "Algorithm for implementing an ABCD ray matrix wave-optics propagator," *Proc. SPIE* **6675**, 66750G (2007).
18. S. Abado, S. Gordeyev, and E. Jumper, "Two-dimensional high-bandwidth shack-hartmann wavefront sensor: design guidelines and evaluation testing," *Opt. Eng.* **49**(6), 064403 (2010).
19. C. Porter et al., "Flight measurements of the aero-optical environment around a flat-windowed turret on the Airborne Aero-Optics Laboratory," *Opt. Eng.* **52**(7), 071404 (2013).

Eric J. Jumper is a professor in the Department of Aerospace and Mechanical Engineering at the University of Notre Dame. His PhD (1975) is in gas dynamics and laser physics from the Air Force Institute of Technology. Since the mid-1990s he has directed the Aero-Optics Group within Notre Dame's Institute for Flow Physics and Control (FlowPAC); the AAOL is one of the research programs in the Aero-Optics Group. He has published more than 50 papers in the area of Aero-Optics.

Michael A. Zenk received his BS (1978) in civil engineering from the United States Air Force Academy. He received a MA (1987) in pastoral ministry from Loyola University (New Orleans) and a MS (1989) in operations research from the Air Force Institute of Technology. He was the operational program manager for the AAOL from Aug 2007 to Feb 2012. Prior to joining the AAOL team, he served in various positions throughout the world as a pilot in the US Air Force. He currently helps direct the financial management of research for the University of Notre Dame's Office of Research, but maintains his interest in all types of airborne research efforts.

Stanislav Gordeyev is a research associate professor at Department of Aerospace and Mechanical Engineering, University of Notre Dame. He is an internationally recognized expert in investigating optical distortions caused by compressible turbulent flows around airborne systems. His expertise includes performing complex experimental investigations of optical aberrations, both in a time-averaged and instantaneous sense, in boundary layers, shear layers and wakes, as well as around complex geometries, like side-mounted turrets at subsonic and transonic speeds; experimental results and developed models are currently widely used to design laser airborne systems, as well to validate computational codes to predict optical distortions caused by turbulent flows. He is also actively involved in various studies of different mitigation techniques to improve the overall optical performance of airborne systems.

David Cavalieri is a research specialist in the Department of Aerospace and Mechanical Engineering of the University of Notre Dame. He has performed project management for the aero-optics group of the Institute for Flow Physics and Control at Notre Dame. He holds dual MS degrees in Aerospace and mechanical engineering from the Illinois Institute of Technology, with a minor in Thermal Analysis. He is a certified professional engineer, specializing in mechanical, and has 20 years of experience in industry and academic research.

Matthew R. Whiteley received his MS (1995) and PhD (1998) in physics from the Air Force Institute of Technology. He received a BS in physics from Carnegie Mellon University in 1991. From 1998 to 2002, he was a deputy chief and advanced concepts team lead at the Airborne Laser Technology Branch of the U.S. Air Force Research Laboratory. From 2002 to 2005, he was a group leader and senior research scientist at ATK Mission Research, and he is now a vice president and senior scientist at MZA Associates Corporation. His research interests include optical turbulence, aero-optical flow, adaptive optics, and wave-optics simulations.